Direct measurement of the nanomechanical stability of a redox protein active site and its dependence upon metal binding

Marina I. Giannotti[a,b,c,*,‡], *Israel Cabeza de Vaca*[d,‡], *Juan M. Artés*[b,c,†], *Fausto Sanz*[a,b,c], *Victor Guallar*[d,e] *and Pau Gorostiza*[a,c,e,*]

a. Networking Biomedical Research Center on Bioengineering, Biomaterials and Nanomedicine (CIBER-BBN), Madrid, 28029, Spain

b. Physical Chemistry Department, Universitat de Barcelona, Barcelona, 08028, Spain

c. Institute for Bioengineering of Catalonia (IBEC). Baldiri Reixac 15-21, Barcelona, 08028, Spain

d. Joint BSC-CRG-IRB Research Program in Computational Biology, Barcelona Supercomputing Center. Jordi Girona 29, Barcelona, 08034, Spain.

e. Catalan Institution for Research and Advanced Studies (ICREA), Barcelona, 08010, Spain.

ABSTRACT. The structural basis of the low reorganization energy of cupredoxins has long been debated. These proteins reconcile a conformationally heterogeneous and exposed metal-chelating site with the highly rigid copper center required for efficient electron transfer. Here we combine single-molecule mechanical unfolding experiments with statistical analysis and computer simulations to show that the metal-binding region of apo-azurin is mechanically flexible and that high mechanical stability is imparted by copper binding. The unfolding pathway of the metal site depends on the pulling residue and suggests that partial unfolding of the metal binding site could be facilitated by the physical interaction with certain regions of the redox protein.

KEYWORDS: azurin; cupredoxins; force spectroscopy; nanomechanical stability; single molecule.

Introduction

Protein-mediated electron transfer (ET) reactions are essential in many biological processes, such as cellular respiration and photosynthesis.[1,2] At the low electrochemical driving forces found in most biological systems, the extraordinary efficiency of such processes is based on the maximization of the coupling between donor and acceptor and the optimization of the reorganization energy.[2-4] Many redox proteins host in their structures transition metal ions like copper and iron, whose electrochemical properties can be tuned by the protein environment to meet the requirements of the biological ET.[5] In iron centers, rigid cofactors like the heme group are used to avoid high reorganization energies when cycling between the geometries preferred by the metal in the different redox states.[5] In contrast, copper ions are bound directly to flexible protein residues, and the rigidity relies upon the protein folding. The entatic/rack-induced state model[6,7] suggests that a metal chelating site is preformed in the protein to impart rigidity regardless of the presence of the ion, in agreement with the virtually identical structure of holo- and apo-cupredoxins[8,9] and the minimized conformational changes during Cu^{II}/Cu^{I} redox cycling.[10]

These views were challenged by the discovery of copper metallochaperones,[11] which load the metal ion into cupredoxins following a mechanism that requires an exposed metal-binding site and protein-protein interactions[12] that are incompatible with a hidden, rigid metal site. In addition, structural evidences of conformational heterogeneity of the metal binding site in cupredoxins[13-15] suggest that the metal binding may contribute to their rigidity and that flexibility in the chelating site may be essential for metallochaperone-mediated copper binding *in vivo*. However, no direct evidence on the mechanical stability of the protein[16] and its relation to the coordination site has yet been reported. The mechanical lability[17] of metal-protein bonds has a

major relevance for the structure and function of redox metalloproteins but it is difficult to characterize using classical structural techniques and thermal or chemical denaturation methods. In order to directly measure the mechanical properties of the Cu-binding region of a cupredoxin and to assess the effect of the metal, we have mechanically unfolded individual azurin (Az) molecules using single molecule force spectroscopy (SMFS) with an atomic force microscope (AFM).[16,18-23] In particular, we compared the holo and apo forms of Az (with and without the Cu ion, respectively) using force-extension curves, statistical analysis and computational simulations. Protein unfolding experiments mediated by mechanical force (SMFS) constitute kinetic rather than thermodynamic measurements, and therefore mechanical unfolding pathways may differ from chemical unfolding ones.[24,25] However, SMFS provides useful insights on protein structure-activity relationships and on the physiological interaction between protein partners that complement those results obtained by *in vitro* denaturation experiments using non-physiological temperatures or chemical agents like urea.

Results and discussion

Mechanical unfolding of individual holo and apo-Az: single molecule force spectroscopy

Holo- and apo-Az display nearly identical tertiary structure[8,9] and thus provide an opportunity to directly determine the role of the metal in Az mechanical stability using AFM-SMFS. We chose wildtype monomeric Az for several reasons, despite the difficulty of the recordings and data analysis compared to multidomain proteins often used in SMFS. Monomers are more biologically relevant and enable a direct comparison with bulk experiments performed with cupredoxins. In addition, using wildtype monomeric Az allows avoiding structural alterations introduced by molecular handles, domain-domain interactions and aggregation problems of multidomain proteins. In order to orient the Cu site of Az toward the AFM probe, we

chemisorbed the protein on an atomically-flat gold surface via native cysteine residues (Cys3 and Cys26)[26,27] and we performed force spectroscopy experiments in buffer solution.

To perform SMFS experiments, the tip of a flexible AFM cantilever was approached to the surface and attached non-specifically to the protein. Unfolding force-extension profiles were recorded upon tip retraction, until the tip-protein contact was ruptured at force F_r and length l_r, both for holo- and apo-Az (Figure 1). Because the interaction between the protein and the AFM tip is non-specific, the tip can make contact and "grab" the protein from different solvent-exposed residues along the chain, and thus different portions of the protein can be stretched and unfolded. The force-extension traces were normalized by the extension corresponding to 110 pN and 150 pN for holo-Az and for apo-Az data sets, respectively. Different normalized force curves for each data set can be superimposed, confirming that single molecules are being stretched (Figure S1). The contact between the probe and holo-Az is ruptured at l_r around 8 nm, while values of l_r are distributed more broadly for apo-Az (5-30 nm, Figure 2a). The distribution of rupture forces F_r is similar in both cases, indicating that the tip-protein interactions are comparable. As the tertiary structure of holo-Az and apo-Az are nearly identical, the differences in l_r recorded values may only indicate that the presence of the copper ion changes the mechanical properties of individual Az proteins. Apo-Az is easier to stretch and unfold and the variation in l_r reflects that the protein is picked up and extended from different residues. In contrast, the maximum extension of holo-Az stays around 8 nm for forces up to 300-400 pN, regardless of the pulling residue. As a control we used denatured Az (den-Az) and representative force-extension plots are displayed in Figure 3a. The probability of stretching den-Az from diverse residues along the chain is independent of F_r, with l_r values ranging from 4 to 40 nm (Figure 3b), in agreement with the total length of the protein.

The forced extension of the unfolding polypeptide chain can generally be described using the worm like chain (WLC) model for polymer stretching.[28] Force-extension curves were fitted to the WLC model (black lines in Figure 1a) to obtain the persistence length l_p and contour length L_c.[29] The WLC model represents a simplified situation in which the force opposed to the elongation of the macromolecule is mainly driven by entropy. However, the apparent persistence length resulting from WLC fits to protein unfolding data from AFM experiments generally reflects a phenomenological stiffness, comprising effects due to both chain entropy and hydrophobic collapse. Typically, l_p values around 0.4 nm are found when the WLC model is used to describe the elastic behavior of proteins.[30-33] For apo-Az, plots of l_p *vs* L_c shown in Figure 2b yield an average l_p value of 0.5 ± 0.3 nm, similar to other polypeptides. In addition, l_p is independent of the maximum force attained during unfolding (Figure 4), which indicates that for apo-Az the mechanical properties obtained from the WLC fit are consistent at all extension values. In contrast, holo-Az curves are not well fitted by the WLC model: l_p displays a wider distribution (0.8 ± 1.2 nm), and a dependence with the rupture force (the highest l_p values were obtained when rupture occurred at low F_r, see Figure 4). In part, this is related to the average stretching length being small to be described by WLC. In addition, these deviations are usually associated with the presence of strong intramolecular interactions that are "softened" upon extension.[34] In holo-Az, these intra-protein interactions must be due to the presence of the metal. Indeed, disruption of these interactions could be the cause of the change in the macromolecular elasticity properties while extension increases, giving rise to broad distribution of l_p values and a dependence on the maximum force attained (F_r). As expected from the l_r values observed, contour lengths L_c are centered on 9 nm for holo-Az and broadly distributed for apo-Az (8-35 nm). Compared to apo- and holo-Az curves, the elastic behavior of den-Az control curves (Figure 3a) was described well by the WLC model, with a value for the average persistence

length of l_p = 0.3 ± 0.1 nm, and contour length L_c up to 45 nm, in accordance with the l_r values obtained experimentally.

In brief, SMFS experiments reveal that apo-Az can be mechanically extended to the total length of the unfolded protein, while holo-Az can be extended to a maximum of approximately 8 nm. Clear deviations of the force-extension from the WLC model for holo-Az indicates the presence of strong intra-protein interactions when the metal is bound. Since the X-ray structures of holo-Az and apo-Az are almost identical, these results demonstrate that the presence of the copper ion increases the mechanical stability of the protein structure at the metallic binding site, and prevents the complete unfolding of holo-Az in SMFS experiments based on non-specific tip-protein interactions (maximum force attained 300-400 pN).

Molecular view of the force-extension differences between apo- and holo-Az: computational simulations

The variability observed in SMFS experiments of Az could not be reduced by increasing the number of experiments, probably due to the concurrence of intrinsically variable conditions like the structural configuration of the protein and the different attachment residues to the AFM tip. In order to gain insight into these variables, we turned to molecular simulations by using the protein energy landscape exploration (PELE; https://pele.bsc.es) software, and calculating the Az unfolding curves from most surface residues (Figure 5). This is the first time that PELE is used to simulate force-extension experiments on protein unfolding (see description of PELE in *Methods*).

In Figure 6 we present example profiles obtained for surface residue Lys128 in holo- and apo-Az simulations. These show that forces in the holo model are higher than in the apo model for a

large fraction of the trajectory. The difference in extension at a constant force is shown in the snapshot (structure of partially unfolded protein) of Figure 6a and is calculated in Figure 7 for the entire range of force. As observed in the holo and apo-Az structure in Figure 6a, while apo-Az is almost fully extended, only part of the holo-Az is unfolded, between the coordination center and the pulling residue (Lys128) for this case. Figure 7a shows the holo and apo-Az difference in extension length between fixed (Cys26) and pulled (gamma carbon of Lys128) atoms for every given force. This difference is highest at 3000 pN, as a result of a shorter extension in holo-Az due to the Cu interaction with its coordinating residues. Figure 7 also includes two snapshots of the atomic representation showing the metal coordination distances before pulling and after the peak for the pulling residue Lys128, and the final snapshot for residues Ala65 (Figure 7b) and Pro75 (Figure 7c) which display a markedly different behaviour.

The expanded view of Figure 6b shows that during holo-Az unfolding, the force increases abruptly at an extension of *ca*. 9 nm, whereas apo-Az unfolds at relatively constant force in this range. This process can be observed in detail in the Supplementary Video S1, and indicates that the strength of the metal–residue interaction stabilizes the difference in extension for a significant force range (or extension time as seen in the Video). Simulations were repeated for all residues shown in Figure 5 and the results are summarized in a force *vs*. length plot (Figure 8) that reproduces the experimental observations of Figure 2a.

Compared to experimental curves, which sample several attachment residues on the protein surface and must be analysed statistically (Figure 2a), in simulations specific residues can be selected to unfold the protein, and unfolding events can be individually tracked. Although calculated force values differ from experimental ones,[35] simulations are not limited by the tip-protein force. Remarkably, both methods fully unfold apo-Az up to 40 nm, whereas holo-Az

unfolding is restricted to (or the simulated force increases steeply at) lengths below 10 nm. The shorter extension in holo-Az is due to the Cu interaction with its coordination residues. For every simulated attachment site, the divergence between the apo- and holo-Az extension is accompanied by strain and eventual rupture of metal coordination bonds in the holo-case (Figure 6b, Figure 7 and Video S1), following different unfolding sequences (as exemplified in Figure 7 for pulling residues Lys128, Pro75 and Ala65). Together, these results indicate that the metal binding region is mechanically flexible when the metal is not coordinated, and Cu coordination prevents the full extension of the protein regardless of the attachment site. Interestingly, the dependence of the unfolding sequence on the pulling residue selected in the simulations suggests that partial unfolding of the metal binding site could be facilitated by the physical interaction with certain regions of the redox protein.

Concluding remarks

In summary, the copper binding site needed for efficient ET in azurin is mechanically flexible in apo-Az, and metal binding increases its mechanical stability. The relevance of the mechanical stability of metal coordination part of the protein for the structure and function of redox metalloproteins is difficult to characterize using classical structural techniques. Our findings suggest that the mechanism of copper loading into cupredoxins may implicate a mechanical contribution, in addition to the well-characterized chemical binding affinity of the metal. [5,36-38]

Methods

Sample Preparation

Native *Pseudomonas Aeruginosa* azurin (holo-Az) and all reagents were purchased from Sigma. Apo-Az was obtained by removing the Cu ion from the protein structure by titrating

holo-Az with a solution 0.1 M KCN, as described.[39] Denatured Az (den-Az) was obtained by keeping holo-Az in 4 M guanidine hydrochloride (GuHCl) solution in acetate buffer (pH 4.5). The apo-Az structure conservation and protein denaturation by GuHCl were followed by monitoring fluorescence from tryptophan Trp48, selectively excited at 290 nm (Figure S2), as the fluorescence maximum of native Az lies at ca. 310 nm and shifts to 350 nm when the protein unfolds.[40] Reported protocols were used to prepare atomically flat gold surfaces[41] and to attach Az on gold[26] through native cysteines Cys3 and Cys26, which results in a defined orientation of the protein on the surface, while preserving its native-like conformation.[42,43] In order to obtain isolated Az molecules on the gold surface, a solution of Az (holo, apo or den) of *ca*. 5 μg mL^{-1} in 50 mM ammonium acetate buffer (pH 4.5) was incubated for 2 h over the substrate and, afterwards, extensively rinsed with buffer solution. All glass-ware used was cleaned with piranha solution (7:3 H_2SO_4:H_2O_2 (30%)). *Caution: Piranha solution should be handled with extreme caution*. Deionized water (18 MΩ cm^{-1} Milli-Q, Millipore) was used to prepare all solutions and for substrate rinsing.

AFM-based single molecule force spectroscopy (SMFS) measurements

SMFS was performed with an MFP-3D AFM (Asylum Research, Santa Barbara, CA). Force curves were acquired using V-shaped Si_3N_4 cantilevers (DNP, Bruker, AFM Probes, Camarillo, CA) with a nominal spring constant of 0.1 N m^{-1}. Individual spring constants were calibrated using the equipartition theorem (thermal noise routine).[44] All the measurements were performed at room temperature in 50 mM ammonium acetate buffer solution, pH = 4.5, previously filtered with 0.02 μm pore filters (Anotop 25 Plus, Whatman) for holo and apo-Az, and in 4 M GuHCl, 50 mM ammonium acetate solution, pH = 4.5, for den-Az. All the experiments were performed in the constant-velocity mode at 1 μm s^{-1} approach and retract velocity.

The experimental results were fitted to a model for single-chain elasticity of random coiled macromolecules, the worm like chain (WLC) model.[29] The model describes a macromolecular chain as a homogeneous string with a constant bending elasticity and predicts the relationship between extension and entropic restoring force generated for a polymer chain. WLC has been effectively used to reproduce the force-extension behavior -at short extensions- of certain synthetic macromolecules[45] and many biomacromolecules, such as DNA[28] and proteins.[46,47] Both l_p and L_c were used as fitting parameters. The force (F) vs. extension (x) interpolation formula of Marko and Siggia[48] was used:

$$\boldsymbol{F(x) = \frac{k_b T}{l_p}\left[\frac{1}{4}\left(1 - \frac{x}{L_c}\right)^{-2} + \frac{x}{L_c} - \frac{1}{4}\right]} \quad (1)$$

PELE computational simulations

PELE is a Monte Carlo method originally developed for exploring the configurational space of protein-ligand recognition. Each Monte Carlo step is composed of three main moves: localized perturbation, side chain sampling and global minimization. The localized perturbation is based on applying anisotropic normal modes (ANM) to the protein in order to describe conformational changes. Additionally, if a ligand is present, it might include its translation and rotation. The second move, side chain sampling, uses rotamer libraries to explore different side chain configurations as a response to the initial local perturbation. Finally, the global minimization optimizes the energy of the newly found configuration. More on PELE can be found in several publications and online: https://pele.bsc.es, where the software is freely available.

We have expanded the code to study single molecule force spectroscopy experiments such as AFM or optical tweezers, in a similar fashion to steered molecular dynamics (SMD).[49] To this aim we have added the possibilities of including atom harmonic constraints to a moving virtual

point (VP). Thus, at each MC step the VP is displaced by a fixed amount in a desired direction. The VP starting position is the same as the restrained atom, giving an initial force of zero. Then, each PELE iteration computes the harmonic force induced by the VP motion, modeling the corresponding force measured by the cantilever. In this study, the lowest 15 ANM modes were chosen, and updated every ten steps. The force constants used in the harmonic VP constraint was set to 10 Kcal/mol·Å^2. Cys3 and Cys26 were fixed with a large harmonic constraint, modeling its surface attachment.

SMD has been largely used to simulate AFM-SMFS experiments in order to obtain an atomic description of unfolding force-extension profiles.[49-51] Monte Carlo methods (such as PELE) are traditionally seen as an alternative to molecular dynamics (MD) techniques. Using PELE, for example, we have recently shown the capability of reproducing protein dynamics at a considerably faster rate than MD.[52] These technological advances open the possibilities of modeling multiple experiments in a timely manner involving, for example, different initial conditions or pulling residues. In order to validate our new approach with an established technique, such as SMD, we also performed SMD simulations for Lys128. See Supporting Information for SMD simulation set up details. As seen in Figure S3, SMD provides the same results as PELE but at the expense of approximately five times higher CPU cost.

System setup. The crystal structure 4AZU[8] was selected from the protein data bank for the computational simulations. The system was prepared with the Protein Preparation Wizard tool,[53] adding missing hydrogen atoms, fixing environment dependent protonation states and checking disulfide bonds. PELE uses the OPLSAA[54] force field with an implicit surface generalized solvent model. The charge of the Cu ion was set to +2. The ionic strength has been set to 0.15 mol dm^{-3}.

From experimental SMFS it is not possible to determine which residue is attached to the cantilever. For this reason, each simulation was performed with a randomly selected residue (to be pulled) from a surface list. The surface residues included: Gln12, Met13, Leu33, Asn38, Leu39, Lys41, Asn42, Val43, Ala54, Gln57, Val60, Ala65, Asp69, Pro75, Asp76, Asp77, Ser78, Val80, Gly90, Lys92, Ser94, Ser100, Pro115, Gly116, Ala119, Leu120, Lys122, Thr124, Thr126, Lys128 (Figure 5). Additionally, the atom to be restrained was chosen randomly between the carbons of the side chain.

Data analysis. Three independent trajectories were performed for each selected residue and state. Then, the average force with respect to the extension was linearly interpolated in order to obtain a continuum force plot. The force peak corresponding to the largest difference in extension between the holo and apo-Az simulations was then selected as an indication of the "rupture force" (Figure 7a). Thus, for each residue there are three pairs of points in Figure 8 (each pair containing one apo and one holo point). Notice that by using this "rupture force", instead of a fixed rupture force, we obtain possibly an upper bound value for the differences between apo and holo.

ASSOCIATED CONTENT

Supporting Information. Supplementary Figures on validation of single molecule force spectroscopy experiments; characterization of denatured azurin; molecular view (computational simulations) of the force-extension: comparison between SMD and PELE, and supplementary Video. This material is available free of charge via the Internet at http://pubs.acs.org.

AUTHOR INFORMATION

Corresponding Author

*Corresponding authors: E-mail: migiannotti@ub.edu (M.I.G.), pau@icrea.cat (P.G.).

Present Addresses

†Electrical and Computer Engineering department. University of California Davis, One Shields Ave, 95616 Davis, CA, USA.

Author Contributions

The manuscript was written through contributions of all authors. All authors have given approval to the final version of the manuscript. ‡These authors contributed equally.

Conflict of Interests

Authors declare no conflict of interests.

ACKNOWLEDGMENT

We are grateful to A. Donaire and I. Díez-Pérez for discussions, and to the Catalan government (grant 2014SGR-1251), the Spanish government (grant CTQ2013-43892R) and the European Research Council (PELE ERC-2009-Adg 25027) for financial support.

REFERENCES

(1) Ramirez, B. E.; Malmstrom, B. G.; Winkler, J. R.; Gray, H. B. *Proc. Natl. Acad. Sci. USA* **1995**, *92*, 11949-11951.
(2) Marcus, R. A.; Sutin, N. *Biochim. Biophys. Acta* **1985**, *811*, 265-322.
(3) Gray, H. B.; Winkler, J. R. *Proc. Natl. Acad. Sci. USA* **2005**, *102*, 3534-3539.
(4) Wallrapp, F. H.; Voityuk, A. A.; Guallar, V. *PLOS Comput. Biol.* **2013**, *9*, e1002990.
(5) Winkler, J. R.; Wittung-Stafshede, P.; Leckner, J.; Malmstrom, B. G.; Gray, H. B. *Proc. Natl. Acad. Sci. USA* **1997**, *94*, 4246-4249.
(6) Lancaster, K. M.; Farver, O.; Wherland, S.; Crane, E. J., III; Richards, J. H.; Pecht, I.; Gray, H. B. *J. Am. Chem. Soc.* **2011**, *133*, 4865-4873.
(7) Vallee, B. L.; Williams, R. J. *Proc. Natl. Acad. Sci. USA* **1968**, *59*, 498-505.
(8) Nar, H.; Messerschmidt, A.; Huber, R.; van de Kamp, M.; Canters, G. W. *J. Mol. Biol.* **1991**, *221*, 765-772.
(9) Nar, H.; Messerschmidt, A.; Huber, R.; van de kamp, M.; Canters, G. W. *FEBS Lett.* **1992**, *306*, 119-124.
(10) Malmström, B. G. *Eur. J. Biochem.* **1994**, *223*, 711-718.

(11) Rae, T. D.; Schmidt, P. J.; Pufahl, R. A.; Culotta, V. C.; V. O'Halloran, T. *Science* **1999**, *284*, 805-808.

(12) Banci, L.; Bertini, I.; Cantini, F.; Felli, I. C.; Gonnelli, L.; Hadjiliadis, N.; Pierattelli, R.; Rosato, A.; Voulgaris, P. *Nat. Chem. Biol.* **2006**, *2*, 367.

(13) Ryde, U.; Olsson, M. H. M.; Roos, B. r. O.; De Kerpel, J. O. A.; Pierloot, K. *JBIC J.Biol. Inorg. Chem.* **2000**, *5*, 565-574.

(14) Messerschmidt, A.; Prade, L.; Kroes, S. J.; Sanders-Loehr, J.; Huber, R.; Canters, G. W. *Proc. Natl. Acad. Sci.* **1998**, *95*, 3443-3448.

(15) Zaballa, M. E.; Abriata, L. A.; Donaire, A.; Vila, A. J. *Proc. Natl. Acad. Sci. USA* **2012**, *109*, 9254-9259.

(16) Rico, F.; Rigato, A.; Picas, L.; Scheuring, S. *J. Nanobiotech.* **2013**, *11*, S3.

(17) Zheng, P.; Takayama, S.-i. J.; Mauk, A. G.; Li, H. *J. Am. Chem. Soc.* **2012**, *134*, 4124.

(18) Shi, W.; Giannotti, M. I.; Zhang, X.; Hempenius, M. A.; Schönherr, H.; Vancso, G. J. *Angew. Chem. Int. Ed.* **2007**, *46*, 8400.

(19) Nash, M. A.; Gaub, H. E. *ACS Nano* **2012**, *6*, 10735.

(20) Zheng, P.; Wang, Y.; Li, H. *Angew. Chem. Int. Ed.* **2014**, *53*, 14060.

(21) Farrance, O. E.; Paci, E.; Radford, S. E.; Brockwell, D. J. *ACS Nano* **2015**, *9*, 1315.

(22) Van Quaethem, A.; Lussis, P.; Leigh, D. A.; Duwez, A.-S.; Fustin, C.-A. *Chemical Science* **2014**, *5*, 1449.

(23) Giannotti, M. I.; Rinaudo, M.; Vancso, G. J. *Biomacromolecules* **2007**, *8*, 2648.

(24) Jagannathan, B.; Elms, P. J.; Bustamante, C.; Marqusee, S. *Proc. Natl. Acad. Sci. USA* **2012**, *109*, 17820-17825.

(25) Wittung-Stafshede, P. *Acc. Chem. Res.* **2002**, *35*, 201.

(26) Friis, E. P.; Andersen, J. E. T.; Madsen, L. L.; Moller, P.; Ulstrup, J. *J. Electroanal. Chem.* **1997**, *431*, 35-38.

(27) Friis, E. P.; Andersen, J. E. T.; Madsen, L. L.; Bonander, N.; Moller, P.; Ulstrup, J. *Electrochim. Acta* **1998**, *43*, 1114-1122.

(28) Bustamante, C.; Marko, J. F.; Siggia, E. D.; Smith, S. *Science* **1994**, *265*, 1599-1600.

(29) Flory, P. J. *Statistical Mechanics of Chain Molecules*; Interscience: New York, 1969.

(30) Ainavarapu, S. R. K.; Brujic, J.; Huang, H. H.; Wiita, A. P.; Lu, H.; Li, L.; Walther, K. A.; Carrion-Vazquez, M.; Li, H.; Fernandez, J. M. *Biophys. J.* **2007**, *92*, 225.

(31) Walther, K. A.; Gräter, F.; Dougan, L.; Badilla, C. L.; Berne, B. J.; Fernandez, J. M. *Proc. Natl. Acad. Sci. USA* **2007**, *104*, 7916-7921.

(32) Carrion-Vazquez, M.; Oberhauser, A. F.; Fowler, S. B.; Marszalek, P. E.; Broedel, S. E.; Clarke, J.; Fernandez, J. M. *Proc. Natl. Acad. Sci. USA* **1999**, *96*, 3694-3699.

(33) Oberhauser, A. F.; Marszalek, P. E.; Erickson, H. P.; Fernandez, J. M. *Nature* **1998**, *393*, 181.

(34) F. Oesterhelt; M. Rief; Gaub, H. E. *New J. Phys.* **1999**, *1*, 6.1-6.11.

(35) Rico, F.; Gonzalez, L.; Casuso, I.; Puig-Vidal, M.; Scheuring, S. *Science* **2013**, *342*, 741-743.

(36) Pozdnyakova, I.; Wittung-Stafshede, P. *J. Am. Chem. Soc.* **2001**, *123*, 10135-10136.

(37) Wittung-Stafshede, P. *Inorg. Chem.* **2004**, *43*, 7926-7933.

(38) Alcaraz, L. A.; Gómez, J.; Ramírez, P.; Calvente, J. J.; Andreu, R.; Donaire, A. *Bioinorg. Chem. Appl.* **2007**, *2007, Article ID 54232*, 1-9.
(39) Fuentes, L.; Oyola, J.; Fernández, M.; Quiñones, E. *Biophys. J.* **2004**, *87*, 1873-1880.
(40) Huang, Q.; Quinones, E. *Arch. Biochem. Biophys.* **2008**, *477*, 175-182.
(41) Nagy, G.; Wandlowski, T. *Langmuir* **2003**, *19*, 10271-10280.
(42) Pompa, P. P.; Bramanti, A.; Maruccio, G.; Cingolani, R.; De Rienzo, F.; Corni, S.; Di Felice, R.; Rinaldi, R. *J. Chem. Phys.* **2005**, *122*.
(43) Ron, I.; Sepunaru, L.; Itzhakov, S.; Belenkova, T.; Friedman, N.; Pecht, I.; Sheves, M.; Cahen, D. *J. Am. Chem. Soc.* **2010**, *132*, 4131.
(44) Proksch, R.; Schaffer, T. E.; Cleveland, J. P.; Callahan, R. C.; Viani, M. B. *Nanotechnology* **2004**, *15*, 1344-1350.
(45) Giannotti, M. I.; Vancso, G. J. *ChemPhysChem* **2007**, *8*, 2290-2307.
(46) Fisher, T. E.; Marszalek, P. E.; Fernandez, J. M. *Nat. Struct. Biol.* **2000**, *7*, 719-724.
(47) Rivas-Pardo, J. A.; Alegre-Cebollada, J.; Ramírez-Sarmiento, C. A.; Fernandez, J. M.; Guixé, V. *ACS Nano* **2015**, *Article ASAP*, doi: 10.1021/nn507480v.
(48) Marko, J. F.; Siggia, E. D. *Macromolecules* **1995**, *28*, 8759-8770.
(49) Lu, H.; Isralewitz, B.; Krammer, A.; Vogel, V.; Schulten, K. *Biophys. J.* **1998**, *75*, 662-671.
(50) Lu, H.; Schulten, K. *Proteins: Structure, Function, and Bioinformatics* **1999**, *35*, 453-463.
(51) Krammer, A.; Lu, H.; Isralewitz, B.; Schulten, K.; Vogel, V. *Proc. Natl. Acad. Sci. USA* **1999**, *96*, 1351-1356.
(52) Cossins, B. P.; Hosseini, A.; Guallar, V. *J. Chem. Theory Comput.* **2012**, *8*, 959-965.
(53) Madhavi Sastry, G.; Adzhigirey, M.; Day, T.; Annabhimoju, R.; Sherman, W. *J. Comput. Aid. Mol. Des.* **2013**, *27*, 221-234.
(54) Jorgensen, W. L.; Maxwell, D. S.; Tirado-Rives, J. *J. Am. Chem. Soc.* **1996**, *118*, 11225-11236.

FIGURES

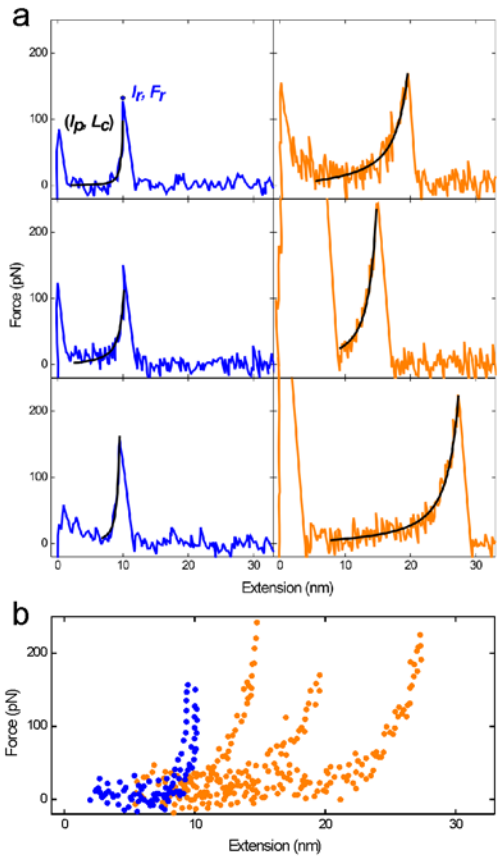

Figure 1. AFM-SMFS force-extension curves. a) Representative AFM-SMFS force-extension traces of individual holo-Az (blue curves) and apo-Az (orange curves) in 50 mM ammonium acetate buffer pH 4.5, at 25 ºC. Black continuous lines in correspond to the fitting of the experimental data to the worm-like chain (WLC) model. b) Superposition of the pulling traces shown in a).

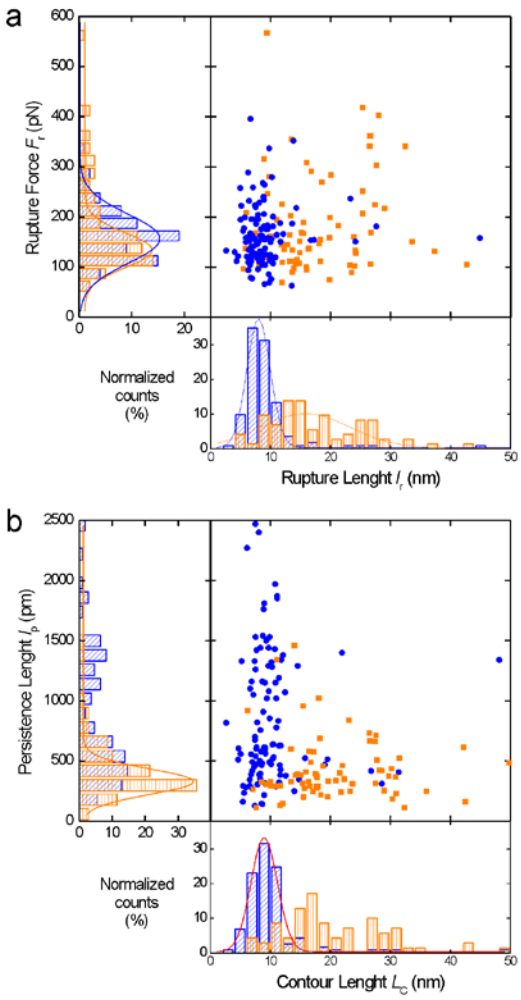

Figure 2. AFM-SMFS and WLC model. Distribution of: a) rupture force (F_r) and length (l_r); b) persistence (l_p) and contour length (L_c) parameters obtained from fitting the experimental data to the WLC model, for AFM-SMFS of individual holo-Az (blue) and apo-Az (orange) in 50 mM ammonium acetate buffer pH 4.5, at 25 ºC.

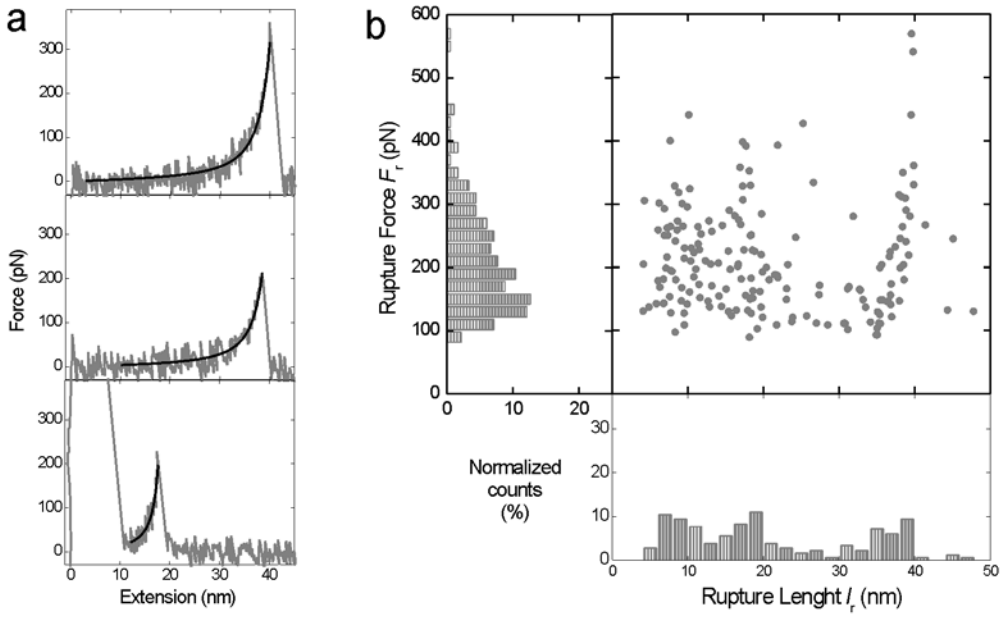

Figure 3. AFM-SMFS on den-Az. a) Representative AFM-SMFS force-extension traces of individual den-Az in 4 M GuHCl and 50 mM ammonium acetate buffer pH 4.5, at 25 ºC. Black continuous lines correspond to the fitting of the experimental data to the worm-like chain (WLC) model. b) Distribution of rupture forces (F_r) and lengths (l_r) for individual den-Az.

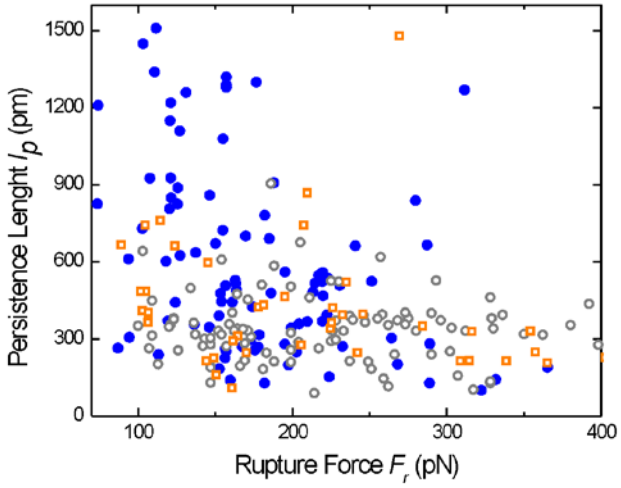

Figure 4. WLC: variation of l_p with F_r. Persistence length (l_p) -obtained from fitting the experimental data to the WLC model- *vs*. rupture force (F_r), for individual holo-Az (blue), apo-Az (orange) (in 50 mM ammonium acetate buffer pH 4.5), and den-Az (gray) (in 4 M GuHCl and 50 mM ammonium acetate buffer pH 4.5, at 25 ºC).

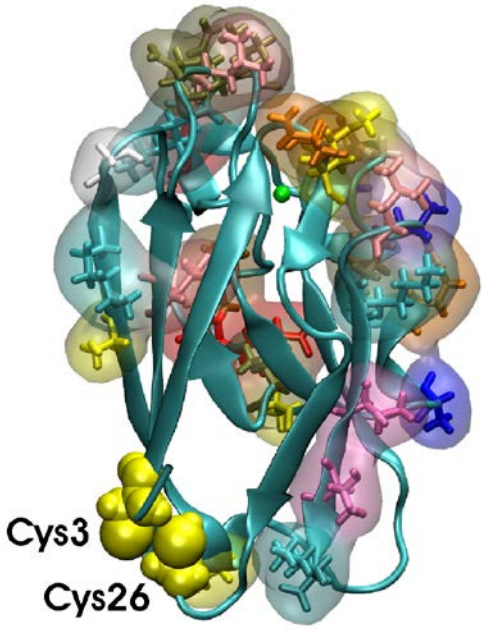

Figure 5. 3D structure of *Pseudomonas aeruginosa* Az where all residues analysed are highlighted. The substrate-attaching residues Cys3 and Cys 26 were fixed in the simulations. The copper ion is represented by a green sphere in the region facing the AFM probe.

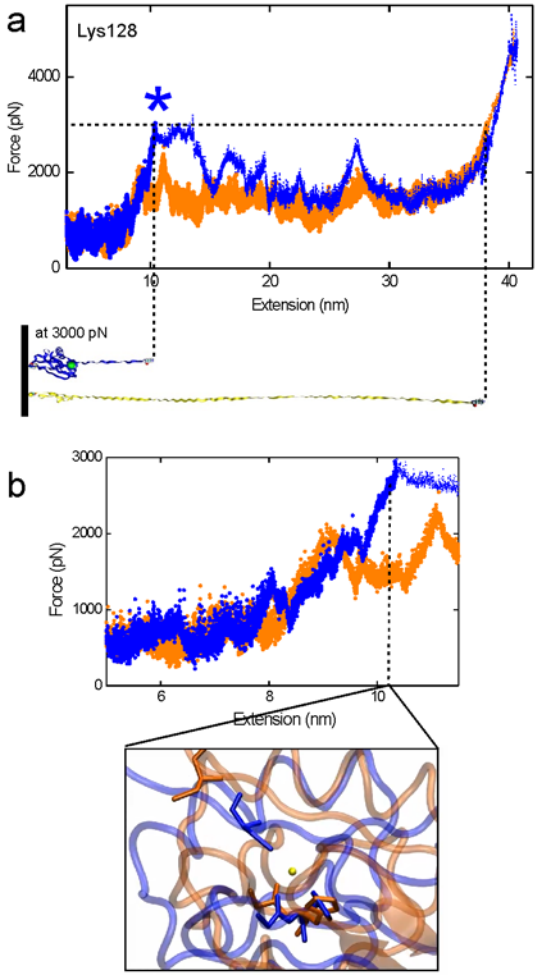

Figure 6. PELE force-extension. a) PELE force-extension profile for surface residue Lys128 of holo-Az (blue) and apo-Az (orange). The asterisk (*) indicates the maximum extension value obtained experimentally for holo-Az. Apo and holo-Az unfolding at the force corresponding to (*) is also displayed. b) Initial stage of unfolding and Cu-binding site conformation snap-shots for holo-Az and apo-Az at 10 nm extension for Lys 128.

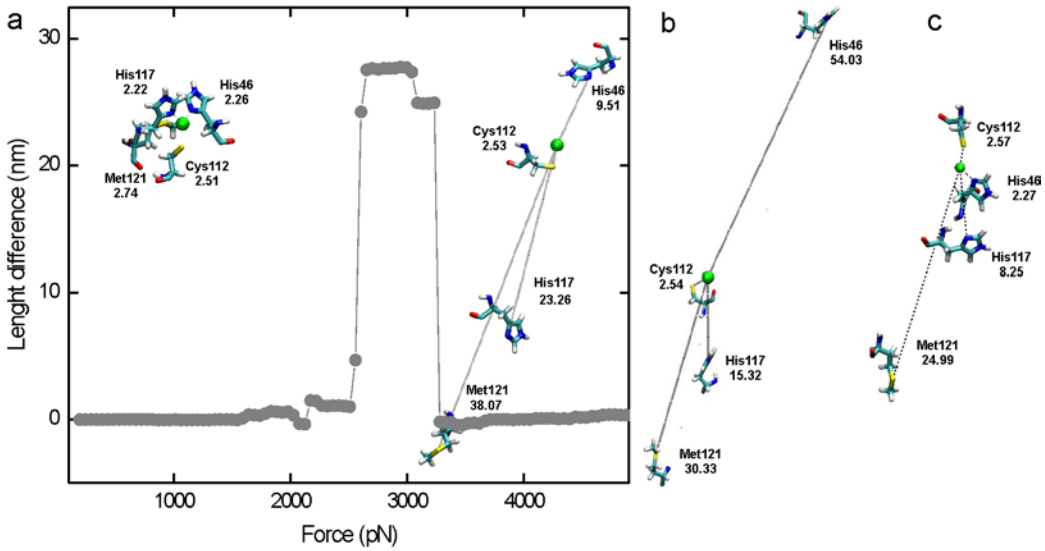

Figure 7. PELE molecular view of the force-extension: a) Difference in extension (length difference) between the holo and apo-Az obtained by PELE at every given force for residue Lys128. Schematics of the distance between the Cu atom and four of its coordination residues (His46, Cys112, His117 and Met121) before and after the maximum force peak at 3000 pN for pulling residues Lys128 (a), Ala65 (b) and Pro75 (c).

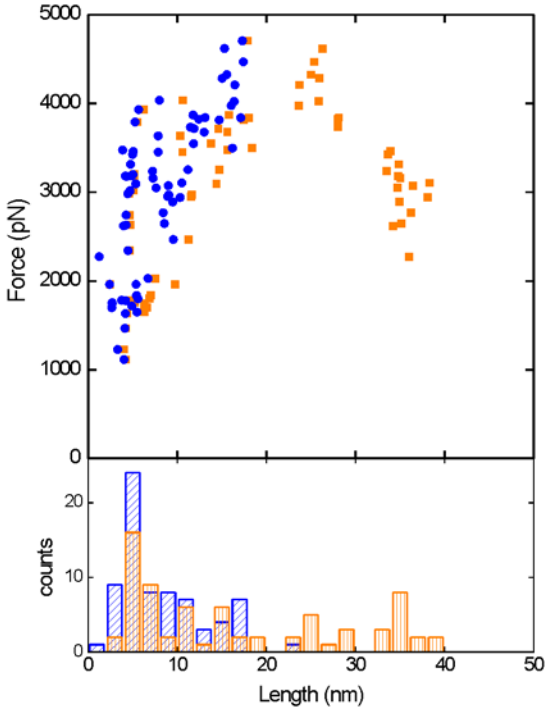

Figure 8. Force *vs*. length obtained from all PELE simulations (see data analysis section) for holo (blue) and apo-Az (orange).

Table of Contents Graphic